ChemComm

COMMUNICATION

View Article Online
View Journal | View Issue

Cite this: *Chem. Commun.*, 2018, **54**, 11765

Received 14th August 2018,
Accepted 25th September 2018

DOI: 10.1039/c8cc06621c

rsc.li/chemcomm

Layer-by-layer preparation of 3D covalent organic framework/silica composites for chromatographic separation of position isomers†

Hai-Long Qian, [abc] Cheng Yang [abc] and Xiu-Ping Yan *[abc]

A layer-by-layer approach was developed to prepare 3D covalent organic framework COF-300/silica composites (COF-300@SiO_2) with uniform morphology as the stationary phase for high performance liquid chromatography separation of position isomers with high efficiency, selectivity and precision.

Crystalline porous material covalent organic frameworks (COFs) constructed from organic monomers with unique features have drawn great concern recently.[1–6] COFs have great potential applications in diverse areas including gas storage,[7] photoconduction,[8,9] sensing,[10,11] and catalysis.[12,13] Moreover, 2D COFs with high stability, unique ordered structures and various functions have played dominant roles in the application of separation sciences,[14] such as sample pretreatment,[15,16] gas chromatography,[17] capillary electrochromatography,[18] and high performance liquid chromatography (HPLC).[19–22] Separation of position isomers is of great significance for their wide application in chemical and pharmaceutical industries,[23] but remains challenging due to their similarity in physicochemical properties. Although COFs have been used as stationary phases for chromatography, baseline separation of position isomers has not achieved on COFs yet.[22]

Exploring the potential of 3D COFs with complicated structures and functions in the separation of position isomers is of great importance both in materials and separation sciences. However, the irregular morphology and wide particle size distribution of bulky COFs give rise to the problems of high backpressure and low column efficiency in their direct application as stationary phases for HPLC. Silica based composites have wide applications for the combined benefits of different materials.[24–26] Growing a uniform COF shell on silica microspheres (SiO_2) is a promising way to resolve the above problems. Direct mixing of substrates such as Al_2O_3, SiO_2 and Fe_3O_4 into the pre-polymerized precursors of COFs is the main way to prepare COF composites.[21,27,28] However, the difficult isolation of the composites from excessive COFs is the major limitation of this method. The layer-by-layer (LBL) approach is a simple and versatile strategy to assemble various composites with high quality.[29,30] Since the substrate separately reacts with the precursors, no isolation is needed for the composites prepared *via* the LBL approach. Nevertheless, the application of the LBL approach for the fabrication of COF composites has not been reported so far.

Herein, we report an LBL approach to fabricate uniform 3D COF-300@SiO_2 composites as the stationary phase for HPLC separation of position isomers. The excellent solvent stability, high surface area and permanent porosity of the imine-linked 3D COF COF-300 [31] make it have great potential as the stationary phase for HPLC.

Typically, COF-300 was prepared under solvothermal (ST) conditions with high temperature and pressure, which is unfavorable for the LBL assembly of high-quality COF-300@SiO_2. The amorphous-to-crystalline transformation approach[32] can avoid the ST process during the assembly of COF composites. Thus, we firstly verified the preparation of COF-300 *via* amorphous-to-crystalline transformation (ESI†).

The main powder X-ray diffraction (PXRD) peaks of the as-prepared COF-300 (Fig. 2a) coincide with those of the COF-300 prepared with the reported ST approach.[31] Fourier transform-infrared spectra (FTIR) of the prepared COF-300 show the appearance of a C=N peak at 1620 cm^{-1} and the absence of some peaks of the starting materials (N–H at 3165 cm^{-1} and 3394 cm^{-1}, C=O at 1689 cm^{-1}) (Fig. S1, ESI†), indicating the formation of imine bonds. Scanning electron microscopy (SEM) and transmission electron microscopy (TEM) images reveal the typical oblong morphology of the as-prepared COF-300 (Fig. S2 and S3, ESI†). The Brunauer–Emmett–Teller (BET) surface area and pore size of COF-300 are 1033 m^2 g^{-1} and *ca.* 7.94 Å, respectively (Fig. S4, ESI†). All the above results indicate the successful preparation of COF-300 *via* amorphous-to-crystalline transformation.

[a] *State Key Laboratory of Food Science and Technology, Jiangnan University, Wuxi 214122, China. E-mail: xpyan@jiangnan.edu.cn*
[b] *International Joint Laboratory on Food Safety, Jiangnan University, Wuxi 214122, China*
[c] *Institute of Analytical Food Safety, School of Food Science and Technology, Jiangnan University, Wuxi 214122, China*

† Electronic supplementary information (ESI) available: Experimental sections and additional figures and tables. See DOI: 10.1039/c8cc06621c

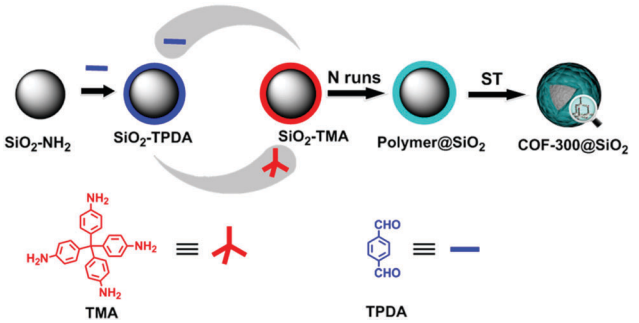

Fig. 1 Scheme for the preparation of COF-300@SiO_2 *via* LBL.

The PXRD pattern of the as-prepared COF-300 did not change in different solvents such as water, methanol, ethanol and acetonitrile (ACN), indicating the possibility of COF-300 for HPLC application (Fig. S5, ESI†).

The LBL approach for the preparation of COF-300@SiO_2 started with refluxing aminosilica (SiO_2–NH_2) with terephthaldehyde (TPDA) to obtain SiO_2–TPDA. The SiO_2–TPDA was subsequently refluxed with tetra(4-anilyl)methane (TAM) to obtain SiO_2–TAM. After repeating the above operation for several cycles, the ploymer@SiO_2 was obtained. Then, a ST process was applied to transfer the amorphous polymer on SiO_2 into ordered COF-300 (Fig. 1).

The PXRD patterns show no main COF-300 characteristic peaks until 3 reaction runs. The main characteristic peaks gradually appeared with the increase of the reaction runs (Fig. 2a). The FTIR spectra also reveal the increase in the intensity of the characteristic peaks at 2919 cm^{-1}, 1620 cm^{-1} and 1491 cm^{-1} (corresponding to the C–H stretching of imine, C=N stretching of imine and the C–C stretching of phenylene–dimethylidene ring, respectively) with the reaction runs (Fig. 2b). Solid-state ^{13}C cross-polarization magic angle spinning nuclear magnetic resonance spectra of the composite are in good agreement with the chemical structure of COF-300, indicating the successful formation of COF-300 on SiO_2 (Fig S6, ESI†). SEM images clearly show the increase in the amount of COF-300 attached on SiO_2 with the reaction runs (Fig. 2c–f and Fig. S7, ESI†). All the results prove the successful preparation of COF-300@SiO_2 as well as the control of the amount of COFs on the surface of SiO_2 by adjusting the reaction runs.

Thermogravimetric analysis (TGA) showed that the COF-300 and its composites remained stable up to 450 °C under N_2 conditions (Fig. S8, ESI†). N_2 adsorption–desorption experiments (Fig. 2g and h) revealed that COF-300@SiO_2 gave a higher BET surface area (431 $m^2\ g^{-1}$) than SiO_2–NH_2 (176 $m^2\ g^{-1}$) due to the presence of the COF-300 (1033 $m^2\ g^{-1}$) on SiO_2. COF-300@SiO_2 exhibited two types of pores with pore sizes of 8.01 Å and 131.45 Å, corresponding to those of COF-300 (7.94 Å) and SiO_2–NH_2 (134.74 Å), respectively.

Van Deemter curves were plotted to evaluate the column efficiency (Fig. S9, ESI†).[33] Compared with the SiO_2–NH_2 packed column (2484 plates per m, corresponding to 402.5 μm plate height), the highest column efficiency of the 3-run COF-300@SiO_2 column for toluene increased to 114 28 plates per m

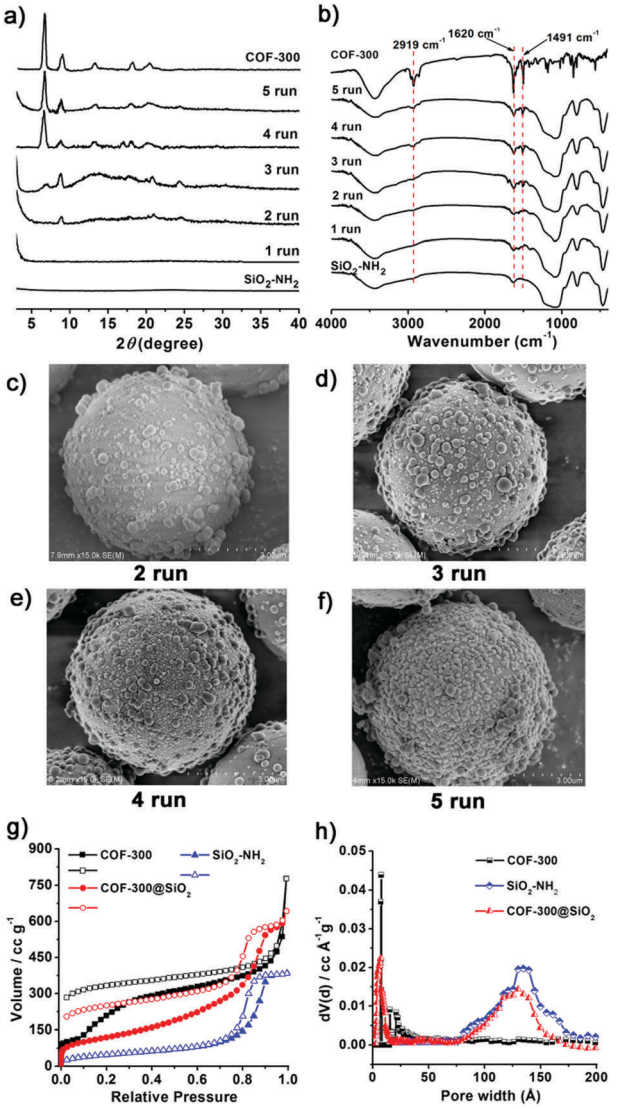

Fig. 2 (a) PXRD patterns and (b) FTIR spectra of COF-300@SiO_2 with different reaction runs. (c–f) SEM images of COF-300@SiO_2 with different reaction runs: (c) 2 runs, (d) 3 runs, (e) 4 runs, and (f) 5 runs. (g) N_2 adsorption–desorption isotherms and (h) pore size distribution curves of COF-300, SiO_2–NH_2 and COF-300@SiO_2.

(87.5 μm plate height), indicating that COF-300 evidently enhanced the performance of the silica column. The 4-run COF-300@SiO_2 column has similar highest column efficiency (23 697 plates per m, 42.2 μm) to the 5-run COF-300@SiO_2 column (25 252 plates per m, 39.6 μm). The column efficiency is mainly affected by the morphology and mass transfer, which is reflected in the Van Deemter coefficients (Table S1, ESI†).[34] The smaller C-term of COF-300@SiO_2 than that of the SiO_2–NH_2 column reveals the faster mass transfer between the analyte and the stationary phase COF-300@SiO_2. A further increase of the reaction run to 5 led to little increase of the C-term. Meanwhile, the decrease in uniformity of the composites with 5 reaction runs resulted in an increase of the A-term. Thus, the increase of the 5-run COF-300@SiO_2 column efficiency seemed not to be obvious. Finally, the 4-run COF-300@SiO_2 column was used in further experiments.

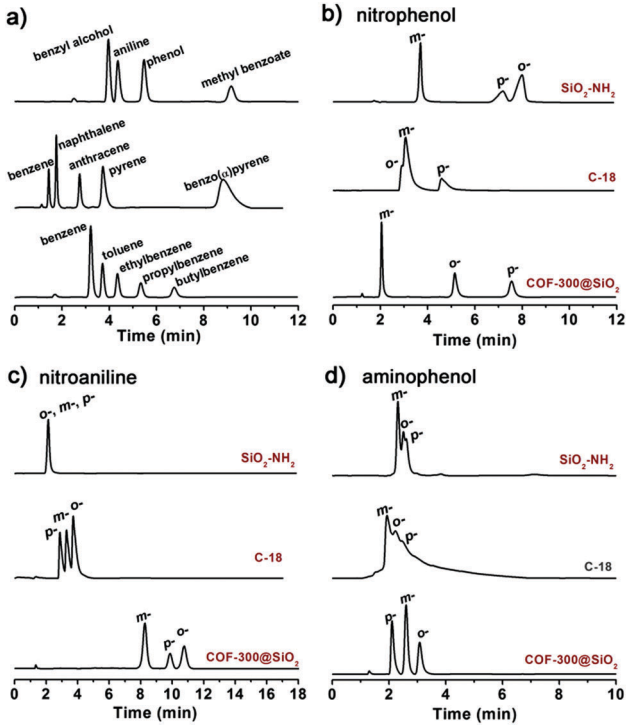

Fig. 3 HPLC chromatograms: (a) benzene homologue, PAHs, substituted aromatics on the COF-300@SiO_2 packed column (15 cm × 4.6 mm i.d.); (b) *o*-, *m*-, *p*-nitrophenol on COF-300@SiO_2, C_{18} and SiO_2 packed columns (15 cm × 4.6 mm i.d.); (c) *o*-, *m*-, *p*-nitroaniline on COF-300@SiO_2, C_{18} and SiO_2 packed columns (15 cm × 4.6 mm i.d.); (d) *o*-, *m*-, *p*-aminophenol on COF-300@SiO_2, C_{18} and SiO_2 packed columns (15 cm × 4.6 mm i.d.). Mobile phase and flow rate: ACN/H_2O (45/55, v/v) and 1.0 mL min^{-1} for the benzene homologue in (a), ACN/H_2O (70/30, v/v) and 1.5 mL min^{-1} for PAHs in (a), ACN/H_2O (30/70, v/v) and 1.0 mL min^{-1} for substituted aromatics in (a), ACN/H_2O (25/75, v/v) and 1.5 mL min^{-1} for (b), ACN/H_2O (20/80, v/v) and 1.5 mL min^{-1} for (c), ACN/H_2O (30/70, v/v) and 1.0 mL min^{-1} for (d); UV detection: 210 nm for (a) and (d), 230 nm for (b), and 254 nm for (c).

Five benzene homologues were baseline separated on the COF-300@SiO_2 column with ACN/H_2O (45/55, v/v) within 7 min (Fig. 3a). The elution of the five analytes is consistent with the C_{18} column (Fig. S10, ESI†) in the order of the hydrophobicity (Table S2, ESI†). Moreover, the effect of ACN on the retention factors (k') further indicates the reversed-phase separation mechanism for the separation of benzene homologues on the COF-300@SiO_2 column (Fig. S11, ESI†). The smaller k' value for the benzene homologue on the COF-300@SiO_2 column compared to that on the C_{18} column reveals the moderate hydrophobicity of the prepared column (Table S3, ESI†).

PAHs including naphthalene, anthracene, pyrene, and benzo(α)pyrene were also baseline-separated on the COF-300@SiO_2 column (Fig. 3a). The elution of PAHs also followed the order of hydrophobicity (Table S2, ESI†). However, naphthalene, anthracene, and pyrene showed much stronger retention than ethylbenzene, butylbenzene and anthracene on COF-300@SiO_2, respectively, although the hydrophobicities of naphthalene, anthracene and pyrene are similar to those of ethylbenzene, butylbenzene and anthracene, respectively. The results indicate additional π–π interaction between the stationary phase and PAHs.

Substituted aromatics such as benzyl alcohol, aniline, phenol and methyl benzoate were also baseline-separated on the COF-300@SiO_2 column (Fig. 3a). In contrast, their baseline separation on the C_{18} column was difficult due to the similar hydrophobicity of benzyl alcohol, aniline and phenol (Fig. S10, ESI†). The opposite elution order of aniline and phenol to their hydrophobicity demonstrates the participation of the hydrogen-bonding interaction. Compared with the C_{18} column, the COF-300@SiO_2 column, due to its weaker hydrophobicity, showed stronger retention of methyl benzoate, indicating the synergism of the van der Waals interactions. No separation of all the above analytes on the SiO_2–NH_2 column further proves the excellent separation performance of the COF-300@SiO_2 column due to the attached COF (Fig. S10, ESI†).

The separation of disubstituted benzene isomers remains a challenge due to their similar properties. Even so, baseline separation of position isomers including *o*-, *m*-, *p*-nitrophenol, *o*-, *m*-, *p*-nitroaniline, and *o*-, *m*-, *p*-aminophenol was achieved on the COF-300@SiO_2 packed column (Fig. 3b–d) with good precision (Table S4, ESI†). The column efficiency of the COF-300@SiO_2 packed column reached 39 593 plates per m for *p*-nitrophenol (Table S5, ESI†). The selectivity factors for the isomers at different temperatures indicate the high selectivity of COF-300@SiO_2 for the analytes (Table S6, ESI†). In contrast, the bare SiO_2–NH_2, SiO_2–NH_2 treated under the same reaction conditions but with no precursors for the 3D COFs, and C_{18} packed columns gave poor resolution for the isomers regardless of the separation conditions, proving that the COF-300 shell plays crucial roles in the separation of isomers (Fig. 3b–d and Fig S12, ESI†). The prepared COF-300@SiO_2 exhibited better separation performance for isomers than other stationary phases including metal–organic frameworks (MIL-53(Al)),[35] molecularly imprinted polymers (MIPs),[36] 2D COF@SiO_2[22] and modified zirconia.[23] In fact, no baseline separation of isomers on MIPs and 2D COF@SiO_2 columns,[22,36] and low column efficiency with tailing and broadening peaks on MIL-53(Al) and modified zirconia column[23,35] were observed.

The separation mechanism of the position isomers was further investigated. Hydrophobic interaction is not the main driving force in the separation of nitrophenol, as the elution order is not in agreement with the hydrophobicity order. The hydrogen-bonding ability of nitrophenol (Table S7, ESI†) with COF-300 determined the resolution. The weakest hydrogen bonding interaction of *m*-nitrophenol with the stationary phase due to its weakest acidity (pK_a = 8.28) led to its first elution. Although the acidities of *o*-nitrophenol (pK_a = 7.23) and *p*-nitrophenol (pK_a = 7.15) are close, the intramolecular hydrogen bond of *o*-nitrophenol decreased its hydrogen bonding with the stationary phase (corresponding to the elution order of *o*- < *p*-).[35–37] The highest hydrophobicity of *o*-nitroaniline among the nitroaniline isomers gave its strongest retention (Table S2, ESI†). The dipolar interaction contributed significantly to the separation of *m*-nitroaniline (dipole moment, 4.89 D) and *p*-nitroaniline (dipole moment, 6.29 D).[23] The same hydrophobicity of *o*-, *m*-, and *p*-aminophenol (Table S2, ESI†) indicates that the hydrophobic interaction was not the driving force for the

resolution of aminophenol isomers (Fig. 3d). The weakest acidity of *p*-aminophenol (Table S7, ESI†) led to its weakest hydrogen bonding ability and weakest retention on COF-300@SiO_2. The driving force for the separation of *o*-aminophenol and *m*-aminophenol with similar acidity is the difference of the van der Waals interactions with the COF-300 stationary phase.

The thermodynamic parameters for the separation of the isomers were obtained from Van't Hoff plots (Fig. S13 and Table S8, ESI†).[38,39] The negative Gibbs free energy change (ΔG) represents the fact that the transfer of isomers from the mobile phase to the stationary phase of COF-300@SiO_2 is thermodynamically spontaneous. The elution of all the position isomers follows a decreasing order of ΔG. The negative value of enthalpy change (ΔH) and entropy change (ΔS) indicates that the retention of the isomers on the COF-300@SiO_2 columns was driven by enthalpy.[40]

In summary, we have developed an LBL approach to fabricate 3D COF@SiO_2 as the stationary phase for HPLC application with COF-300 as a model 3D COF. Several kinds of analytes including benzene homologues, PAHs, and substituted aromatics have been employed to show their various interactions with the prepared stationary phase. Especially, we have demonstrated the excellent performance of COF-300@SiO_2 for the separation of position isomers such as nitrophenol, nitroaniline and aminophenol isomers with high efficiency, selectivity and precision. We have also proposed the separation mechanism of COF-300@SiO_2 for the isomers. This work not only provides a new method for the preparation of COF composites, but also offers new stationary phases for HPLC separation, especially for the separation of isomers.

This work was supported by the National Basic Research Program of China (No. 2015CB932001), the National Natural Science Foundation of China (No. 21775056 and 21804055), the Natural Science Foundation of Jiangsu Province (No. BK20180585), the China Postdoctoral Science Foundation (No. 2018M630510), the National First-Class Discipline Program of Food Science and Technology (No. JUFSTR20180301), and the Fundamental Research Funds for the Central Universities (No. JUSRP11844 and JUSRP51714B).

Conflicts of interest

There are no conflicts to declare.

Notes and references

1 A. P. Côté, A. I. Benin, N. W. Ockwig, M. O'Keeffe, A. J. Matzger and O. M. Yaghi, *Science*, 2005, **310**, 1166–1170.
2 S. Y. Ding and W. Wang, *Chem. Soc. Rev.*, 2013, **42**, 548–568.
3 X. Feng, X. Ding and D. Jiang, *Chem. Soc. Rev.*, 2012, **41**, 6010–6022.
4 P. J. Waller, F. Gandara and O. M. Yaghi, *Acc. Chem. Res.*, 2015, **48**, 3053–3063.
5 J. L. Segura, M. J. Mancheno and F. Zamora, *Chem. Soc. Rev.*, 2016, **45**, 5635–5671.
6 N. Huang, P. Wang and D. Jiang, *Nat. Rev. Mater.*, 2016, **1**, 16068.
7 H. Furukawa and O. M. Yaghi, *J. Am. Chem. Soc.*, 2009, **131**, 8875–8883.
8 H. Xu, S. Tao and D. Jiang, *Nat. Mater.*, 2016, **15**, 722–726.
9 T. Sick, A. G. Hufnagel, J. Kampmann, I. Kondofersky, M. Calik, J. M. Rotter, A. Evans, M. Doblinger, S. Herbert, K. Peters, D. Bohm, P. Knochel, D. D. Medina, D. Fattakhova-Rohlfing and T. Bein, *J. Am. Chem. Soc.*, 2018, **140**, 2085–2092.
10 S. Dalapati, S. Jin, J. Gao, Y. Xu, A. Nagai and D. Jiang, *J. Am. Chem. Soc.*, 2013, **135**, 17310–17313.
11 S. Y. Ding, M. Dong, Y. W. Wang, Y. T. Chen, H. Z. Wang, C. Y. Su and W. Wang, *J. Am. Chem. Soc.*, 2016, **138**, 3031–3037.
12 H. Xu, J. Gao and D. Jiang, *Nat. Chem.*, 2015, **7**, 905–912.
13 C. S. Diercks, S. Lin, N. Kornienko, E. A. Kapustin, E. M. Nichols, C. Zhu, Y. Zhao, C. J. Chang and O. M. Yaghi, *J. Am. Chem. Soc.*, 2018, **140**, 1116–1122.
14 H.-L. Qian, C.-X. Yang, W.-L. Wang, C. Yang and X.-P. Yan, *J. Chromatogr. A*, 2018, **1542**, 1–18.
15 G. Lin, C. Gao, Q. Zheng, Z. Lei, H. Geng, Z. Lin, H. Yang and Z. Cai, *Chem. Commun.*, 2017, **53**, 3649–3652.
16 C. Gao, G. Lin, Z. Lei, Q. Zheng, J. Lin and Z. Lin, *J. Mater. Chem. B*, 2017, **5**, 7496–7503.
17 H.-L. Qian, C.-X. Yang and X.-P. Yan, *Nat. Commun.*, 2016, **7**, 12104.
18 X. Niu, S. Ding, W. Wang, Y. Xu, Y. Xu, H. Chen and X. Chen, *J. Chromatogr. A*, 2016, **1436**, 109–117.
19 W. Zhao, K. Hu, C. Hu, X. Wang, A. Yu and S. Zhang, *J. Chromatogr. A*, 2017, **1487**, 83–88.
20 L.-H. Liu, C.-X. Yang and X.-P. Yan, *J. Chromatogr. A*, 2017, **1479**, 137–144.
21 X. Han, J. Huang, C. Yuan, Y. Liu and Y. Cui, *J. Am. Chem. Soc.*, 2018, **140**, 892–895.
22 K. Zhang, S. L. Cai, Y. L. Yan, Z. H. He, H. M. Lin, X. L. Huang, S. R. Zheng, J. Fan and W. G. Zhang, *J. Chromatogr. A*, 2017, **1519**, 100–109.
23 L. F. Yao, H. B. He, Y. Q. Feng and S. L. Da, *Talanta*, 2004, **64**, 244–251.
24 Y. Imai, A. Kensuke Naka and Y. Chujo, *Macromolecules*, 1999, **32**, 1013–1017.
25 Z. Xie, H. He, Y. Deng, X. Wang and C. Liu, *J. Mater. Chem. C*, 2013, **1**, 1791.
26 J. Sun, B. Yuan, X. Hou, C. Yan, X. Sun, Z. Xie, X. Shao and S. Zhou, *J. Mater. Chem. C*, 2018, **6**, 8495–8501.
27 H. Lu, C. Wang, J. Chen, R. Ge, W. Leng, B. Dong, J. Huang and Y. Gao, *Chem. Commun.*, 2015, **51**, 15562–15565.
28 Y. Li, C.-X. Yang and X.-P. Yan, *Chem. Commun.*, 2017, **53**, 2511–2514.
29 F. X. Xiao, M. Pagliaro, Y. J. Xu and B. Liu, *Chem. Soc. Rev.*, 2016, **45**, 3088–3121.
30 S. Srivastava and N. A. Kotov, *Acc. Chem. Res.*, 2008, **41**, 1831–1841.
31 F. J. Uribe-Romo, J. R. Hunt, H. Furukawa, C. Klöck, M. O'Keeffe and O. M. Yaghi, *J. Am. Chem. Soc.*, 2009, **131**, 4570–4571.
32 J. Tan, S. Namuangruk, W. Kong, N. Kungwan, J. Guo and C. Wang, *Angew. Chem., Int. Ed.*, 2016, **55**, 13979–13984.
33 J. J. van Deemter, F. J. Zuiderweg and A. Klinkenberg, *Chem. Eng. Sci.*, 1956, **5**, 271–289.
34 H. Zhang, J. Ou, Z. Liu, H. Wang, Y. Wei and H. Zou, *Anal. Chem.*, 2015, **87**, 8789–8797.
35 C.-X. Yang, S.-S. Liu, H.-F. Wang, S.-W. Wang and X.-P. Yan, *Analyst*, 2012, **137**, 133–139.
36 X. Huang, L. Kong, X. Li, C. Zheng and H. Zou, *J. Mol. Recognit.*, 2003, **16**, 406–411.
37 B. Koubaissy, G. Joly and P. Magnoux, *Ind. Eng. Chem. Res.*, 2008, **47**, 9558–9565.
38 J. L. Anderson and D. W. Armstrong, *Anal. Chem.*, 2005, **77**, 6453–6462.
39 Y.-Y. Fu, C.-X. Yang and X.-P. Yan, *Chem. – Eur. J.*, 2013, **19**, 13484–13491.
40 E. Küsters, V. Loux, E. Schmid and P. Floersheim, *J. Chromatogr. A*, 1994, **666**, 421–432.

